Issues with Micromagnetic Numerical Simulations of Magnetic Structures of Soft Magnetic Materials for Electric Vehicles

F. Akagi[1]
[1]Dept. of Applied Physics, Kogakuin Univ., Shinjuku 163-8677, Japan

1. Introduction

Ferromagnetic materials are used in the drive motors of electric vehicles. NdFeB magnets are used on the rotating part (or “rotor”) of drive motors and electrical steel is used on the stationary part (or “stator”). In terms of magnetic properties, NdFeB magnets are classified as hard magnetic material and electrical steel as soft magnetic material. Electrical steel has two magnetic characteristics. One is that iron loss (sum of hysteresis and eddy current losses) is low during transformation between electrical and magnetic energies. The other is that high magnetic flux densities are obtained even if low magnetic fields are applied to the soft magnetic materials. We previously reported that we performed micromagnetic numerical simulations of magnetic domain structures in electrical steel [1)]. Calculation models were assumed to be grain-oriented electrical steel (GOES) for transformer cores with an anisotropy field at 20 kA/m. Magnetization reversal in the GOES occurred by applying a DC magnetic field of 8 kA/m. This DC magnetic field was less than half of the anisotropy field but experimentally equals zero, which corresponds to the coercivity (H_c) of the GOES. Therefore, the DC magnetic field used for the micromagnetic numerical simulations was larger than expected. In this report, we describe issues with using electrical steel in simulation models, and we compare MH-loops between soft and hard magnetic materials to clarify what the issues with the micromagnetic numerical simulations for soft magnetic materials are.

2. Micromagnetic numerical simulation

In this simulation, a dynamic magnetic reversal process was calculated using the Landau–Lifshitz–Gilbert equation as follows:

$$\frac{\mathrm{d}M}{\mathrm{d}t} = -\gamma(M \times H_{eff}) + \frac{\alpha}{M_s}\left(M \times \frac{dM}{\mathrm{d}t}\right), \tag{1}$$

where, M is magnetization and M_s is saturation magnetization [2)]. H_{eff} is an effective field, which is the sum of an external, static, anisotropy, and exchange fields. γ is the gyromagnetic ratio and α is the damping factor.

In our calculations of MH-loops, a model of magnetic material contained 16×16×16 cubic cells that were 3 nm long. The M_s was 1.0 T, the intercell exchange stiffness constant was assumed to be 1.0×11^{-11} J/m, and the damping constant was 0.02. The cells have uniaxial magnetic anisotropy, which aligned in one direction. The anisotropy field (H_k) was changed from 10–300 kA/m. The external field was defined by a cosine function, of which the frequency was 25 MHz.

3. Results and discussions

Table 1 compares the magnetic characteristics of soft and hard magnetic materials. Magnetic domain wall width (σ) and exchange length (ρ) are given as

$$\sigma = \pi\sqrt{\frac{A}{K_u}}, \qquad \rho = \sqrt{\frac{A}{K_u}}, \tag{2}$$

where A is the exchange stiffness constant and K_u is the anisotropy constant. The soft magnetic materials are referred to as GOES and non-GEOS; the hard magnetic materials are referred to as NdFeB for motors and CoCr alloy for hard disk drives. The cell sizes of simulation models are defined by exchange length; the cell sizes must be equal to or less than the exchange length for the NdFeB and CoCr alloy. We must consider the cell size and magnetic domain width for

GOES or non-GEOS. The exchange length cannot be calculated and the cell size cannot be determined because the magnetic domain wall width and the exchange stiffness constant are unknown. If the magnetic domain wall width is on the order of 10 nm—which equals 100–150 atoms—the intercell exchange stiffness constant is 2×10^{-13} J/m and the exchange length is about 4.5 nm. Therefore, the cell size should be smaller than 4.5 nm. However, the number of the cell is needed more than 20,000 in the direction of magnetic domain width, because the magnetic domain width is over 100 μm for GEOS. Therefore, simulations of GEOS are very difficult because they are time-consuming and require a lot of memory. As the cell increases in size, simulations of the motions of the magnetic moments in the magnetic domain wall are not precise.

Next, we compared MH-loops between soft and hard magnetic materials to clarify what the issues with the micromagnetic numerical simulations of the soft magnetic materials are. The magnetic materials were assumed to be small, as mentioned in Chapter 2. Figure 1 shows the relationship between H_k and H_c, calculated from MH-loops. The graph in Fig. 1 shows that when the H_k was higher than or equal to 100 kA/m, the H_c was proportional to the H_k. When the H_k was lower than 100 kA/m, the H_c was about 30–40 kA/m. In particular, when the H_k was lower than 20 kA/m, the H_c was larger than H_k. This might be due to the equilibrium between the exchange and static magnetic fields.

We have to solve the above issues in order to simulate soft magnetic materials using a micromagnetic numerical simulation.

Table 1 Comparison of magnetic characteristics of soft and hard magnetic materials.

Magnetic material		Grain size	Magnetic domain width	Magnetic domain wall width (nm)	M_s (T)	K_u (J/m^3)	H_k (kA/m)	Exchange stiffness constant (J/m)	Exchange length (nm)	Cell size (nm)
Soft	GOES	1−2 cm (～10 μm)	> 100 μm	unknown	2	2×10^4	20	unknown	-	-
	Non-GOES		> 10 μm							
Hard	Nd-Fe-B	200−1000 (nm)	-	4.4	1.6	5×10^6	6000	1×10^{-11}	1.4	2
	CoCr alloy	< 10 (nm)	-	10.0	< 1.0	$> 1 \times 10^6$	2000	1×10^{-11}	3.2	1−10

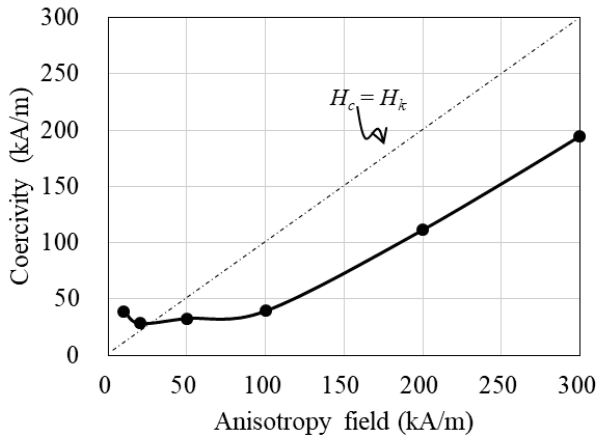

Fig. 1 Anisotropy field dependence of coercivity.

Acknowledgments

We thank Hitachi Corp. for providing us with the use of this simulator.

References

1) F. Akagi, K. Fujisaiki, The Papers of Joint Technical Meeting on “Rotating Machinery” and “Linear Drives” RM-17-045, LD-17-026, 2017, p. 19.

2) F. Akagi, J. Ushiyama, A. Ayano, and H. Miyamoto, “Head and Granular Media for Thermally Assisted Magnetic Recording for Recording Density of 6 Tb/in^2,” *IEEE Trans. on Magn.*,Vol. 49, Issue 7, 2013, p. 5667.

Polycrystalline Magnetic Field Analysis of Electrical Steel for Magnetic Multi-Scale

Keisuke Fujisaki
(Toyota Technological Institute)

Electrical steel is mainly used for electrical motor core or transformer due to high magnetic performance and mass production technology. It is polycrystalline material where each crystal has some magnetic domain with saturated magnetization. So it is said to be an important role between magnetic domain and electrical motor in magnetic multi-scale problem. Usually its calculation model of magnetic analysis should be carried out by magnetic domain model such as LLG or so. However, since electrical steel of polycrystalline has a lot of magnetic domains, when all the magnetic domains are considered for numerical calculation, mesh explosion problem will occur. So the polycrystalline of electrical steel should be modeled to avoid it. Here, static magnetic field analysis in finite element method is used for it in some assumptions that equivalent magnetic material constants are used in homogenized method and coordinate transform of magnetic flux density is used[1-3].

Figure 1 shows total coordinates in polycrystalline and local coordinates in each crystal. Magnetic anisotropy of each crystal is expressed in local coordinate and continuity of magnetic flux density is expressed in total coordinate[4]. So the coordinate transform between them is carried out. GO (grain oriented steel) material with 56 crystal grains in 80 mm^2 square are used for calculation in comparison with the measured magnetic property. Crystal orientations as α, β, γ angles defined in Fig. 1 are well organized and they are centralized within several degrees in average.

Figure 2 shows comparison of magnetic flux density distribution between 3D polycrystalline magnetic field analysis and distributed magnetic measurement[4]. Fig. 2 (a) is measured magnetic flux density by needle method with some square and Fig. 2 (b) is calculation one where magnetic flux density distribution as Fig. 3 (c) is averaged in some square of the needle method. The calculation result well expresses the measured one.

Figure 3 shows comparison of inclination angle of magnetic flux density vector $\vec{B}$ between 3D polycrystalline magnetic field analysis and distributed magnetic measurement[4]. Fig. 3 is the calculated inclination angle which is an angle between the easy magnetization direction of the polycrystalline and the magnetic flux density vector, and Fig. 3 (b) is α angle of each crystal grain. Magnetic flux density is expected to flow in polycrystalline in order to follow each crystal orientation. So angle distribution of Fig. 3 (a) and (b) are in good agreement.

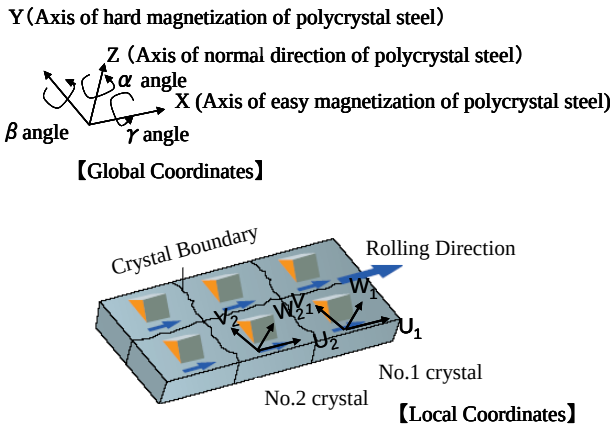

Fig.1. Total coordinates and local coordinates for polycrystalline magnetic field analysis.

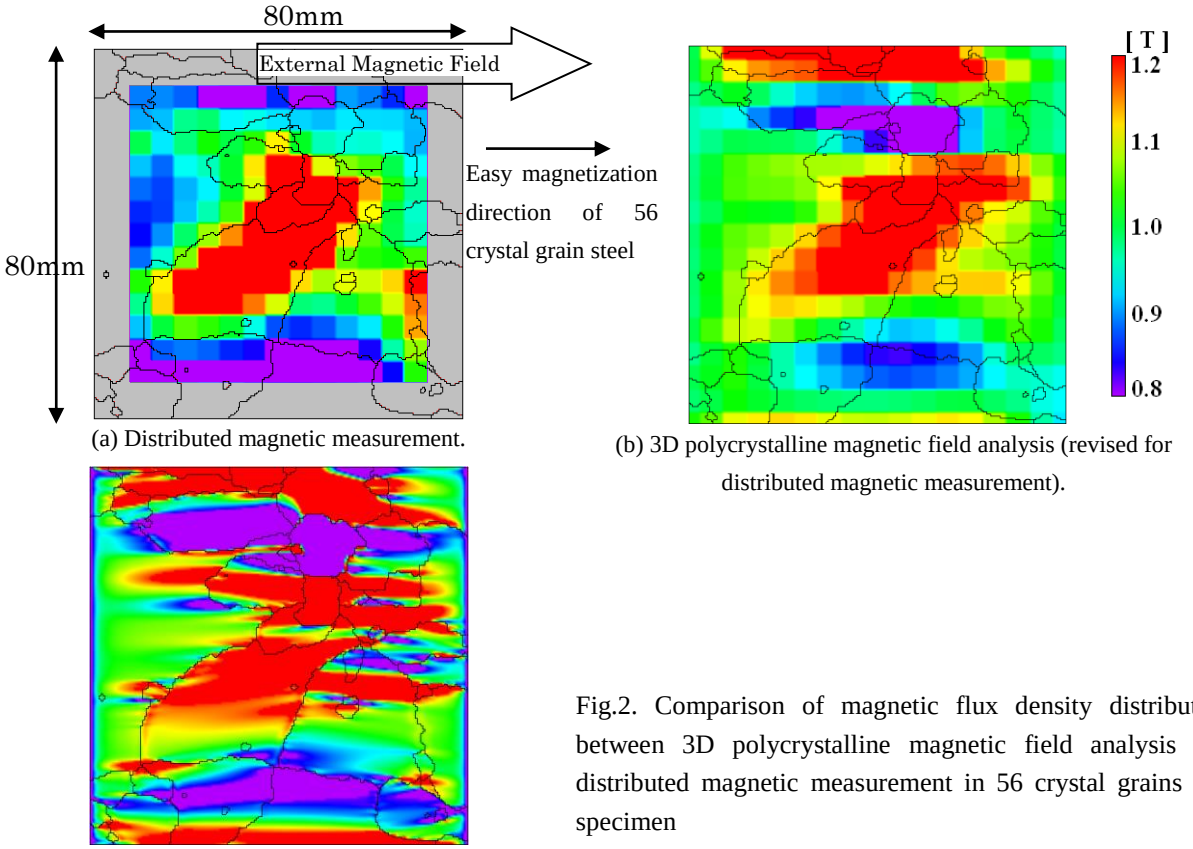

(a) Distributed magnetic measurement.

(b) 3D polycrystalline magnetic field analysis (revised for distributed magnetic measurement).

(c) 3D polycrystalline magnetic field analysis (original).

Fig.2. Comparison of magnetic flux density distribution between 3D polycrystalline magnetic field analysis and distributed magnetic measurement in 56 crystal grains GO specimen

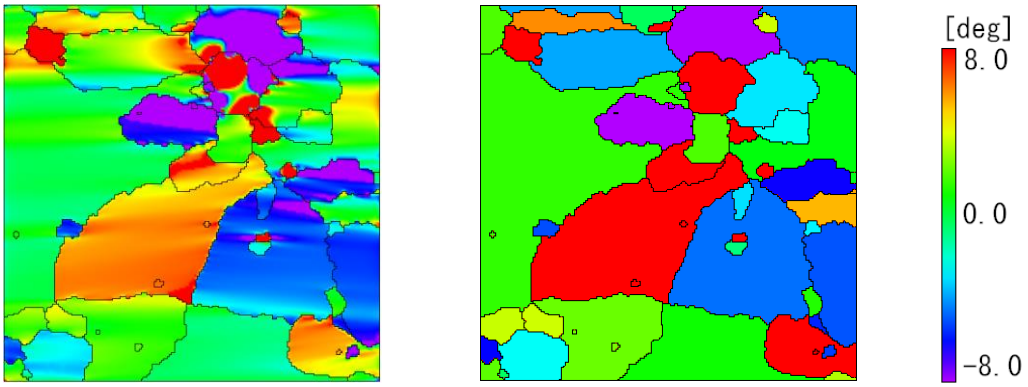

(a) 3D polycrystalline magnetic field analysis

(b) α angle distribution.

Fig.3. Comparison of inclination angle of magnetic flux density vector $\vec{B}$ between 3D polycrystalline magnetic field analysis and distributed magnetic measurement in 56 crystal grains GO specimen.

Reference

1) K. Fujisaki, S. Satoh, “Numerical calculations of electromagnetic fields in silicon steel under mechanical stress,” IEEE Trans. on Magn., Vol. 40, No.4, pp.1820–1825, (2004).
2) K. Fujisaki, M. Fujikura, J. Mino, S. Satou, “3-dimensional Magnetic Field Analysis by Homogenization Method for Thin Steel Plate,” Trans. D, IEEJ, Vol.128, No.3, pp.303-309, (2008).
3) K. Fujisaki, T. Tamaki, “Three-dimensional Polycrystal Magnetic Field Analysis of Thin Steel”, IEEE Transactions on Magnetics s, Volume 45, No.2, pp.687-693, February, (2009).
4) Keisuke Fujisaki, Teruyuki Tamaki, Shouichi Yasuhiro, “Comparison of 3D Polycrtystal Magnetic Field Analysis and Distributed Magnetic Measurement,” Trans. A, IEEJ, vol.129, no.11. pp. 821-826, 2009.

Harmonic Iron Loss Analysis of Rotating Machines: Practical Macro Modeling for Stress and Hysteresis

Katumi Yamazaki
(Chiba Institute of Technology)

In this symposium, I present harmonic iron loss analysis of rotating machines that considers effects of multi-axial mechanical stress and hysteresis phenomenon by introducing practical macro modeling.

First, the effect of the multi-axial stress on the loss is investigated by material experiments. An approximated modeling, which requires only the measured loss with uniaxial stress, is also introduced. Fig. 1 shows the experimental system [1], in which arbitrary 2-axial stress can be imposed on the specimen of an electrical steel sheet by the actuators noted 1 and 2. The magnetic field is applied along the direction of the force produced by actuator 1. The specimen is an electrical steel sheet with 3% silicon.

The hysteresis loss and the eddy current loss including the excess loss are separated from the measured total core losses at 50 Hz and 200 Hz. Fig. 2 shows the results. It is revealed that both the eddy current and hysteresis losses are affected by multi-axial stress. These losses become maximum when the compressive (minus) σ_1 and tensile (plus) σ_2 are imposed.

This experiment cannot be always carried out for practical design procedure of rotating machines. Approximated modeling is strongly desired. To obtain the approximated multi-axial stress effects, the single axial equivalent stress σ_{eq} has been proposed.

Following expression was derived under the assumption that a same magneto-elastic energy leads to a same characteristics of the magnetic materials [2]:

$$\sigma_{eq} = \frac{3}{2}\vec{h}.\boldsymbol{s}.\vec{h} \qquad (1)$$

where $\vec{h}$ is the unit vector along the magnetic field direction, $\boldsymbol{s}$ is the deviatoric part of the stress tensor expressed by σ_1 and σ_2. It is assumed that the variation in core loss with single σ_{eq} along the magnetic field direction is identical to that with multi-axial σ_1 and σ_2. Therefore, the effect of the multi-axial stress can be estimated only by (1) and the experiment, in which a uniaxial stress is simply imposed along the flux direction.

Fig. 3 shows the calculated variation in the losses only from the measured loss $W(\sigma_1,0)$ by single axial σ_1 and the equivalent stresses. It is confirmed that the calculated result well express the measured eddy current and hysteresis losses in Fig. 2.

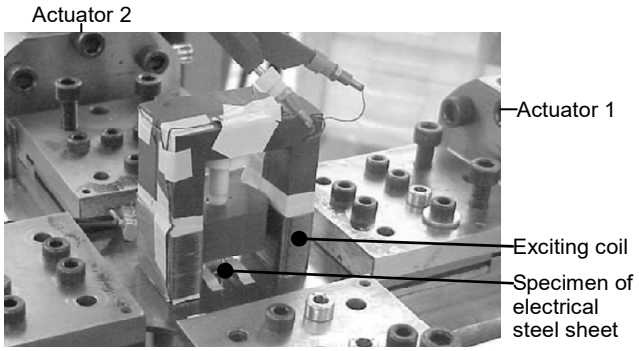

Fig. 1. Experimental system for effect of multi-axial stress[1].

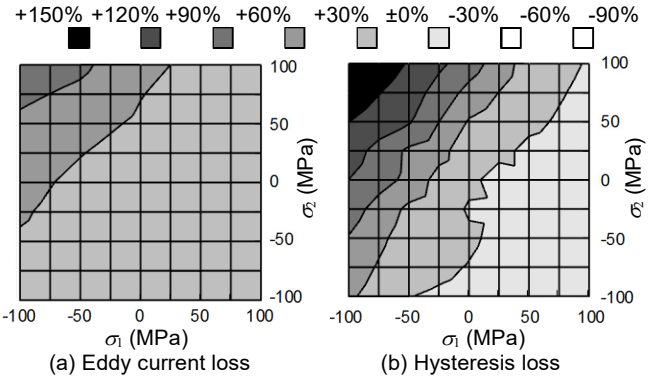

Fig. 2 . Measured variation in losses with multi-axial stress.

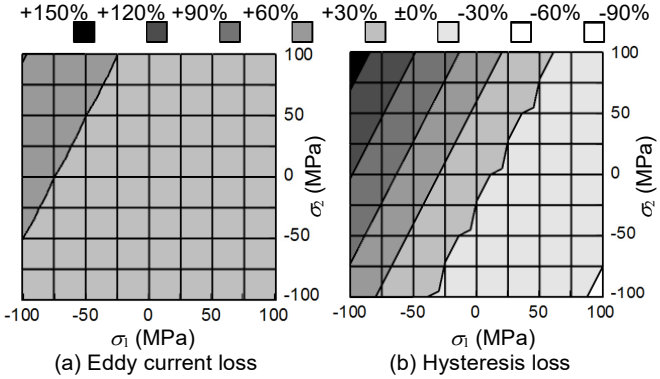

Fig. 3. Calculated losses by $W(\sigma_1,0)$ and σ_{eq} by (1)

Next, a practical hysteresis modeling including minor loops is proposed [3]. Fig. 4 shows the concept of this model. The minor loops are approximately determined form the several curves of major loops. Fig. 5 shows the experimental verification of this model by a single sheet test of an electrical steel sheet. The accuracy of the model is confirmed.

Finally, the proposed material modeling is applied to the loss calculation of a 100 kW class interior permanent magnet synchronous motor driven by a PWM inverter (5 kHz carrier). The 2D finite element analysis is carried out due to following equation.

$$\nabla \times \left(\frac{1}{\mu} \nabla \times \boldsymbol{A} \right) = \nabla \times \boldsymbol{H}_{eddy,ave} + \nabla \times \boldsymbol{H}_{hys,ave} \quad (2)$$

where μ is the permeability, $\boldsymbol{A}$ is the magnetic vector potential, $\boldsymbol{H}_{eddy,ave}$ and $\boldsymbol{H}_{hys,ave}$ are the reation field caused by the eddy currents and hysteresis phenomenon in the core, which are averaged along the thickness of electrical steel sheets. $\boldsymbol{H}_{eddy,ave}$ is determined by coupling 1D nonlinear time stepping analysis along the thickness of the electrical steel sheet in the core. $\boldsymbol{H}_{hys,ave}$ is determined by the presented hysteresis model by considering the effect of the stress due to (1).

Fig. 6 shows the calculated flux density waveform at the top of a stator tooth of the motor. The waveform includes high-frequency carrier harmonics. Fig. 7 shows the calculated hysteresis loops, which includes a considerable number of minor loops. It is observed that the differential permeability of the minor loops is considerably smaller than that of the B-H curve used in the conventional analysis. Fig. 8 shows the experimental and calculated iron losses. The accuracy is improved by the proposed method due to the correct estimation of skin effect.

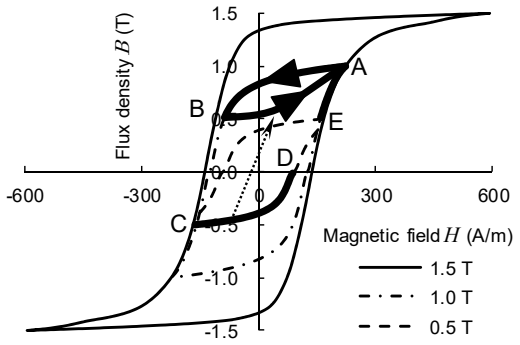

Fig. 4. Minor hysteresis loop modeling.

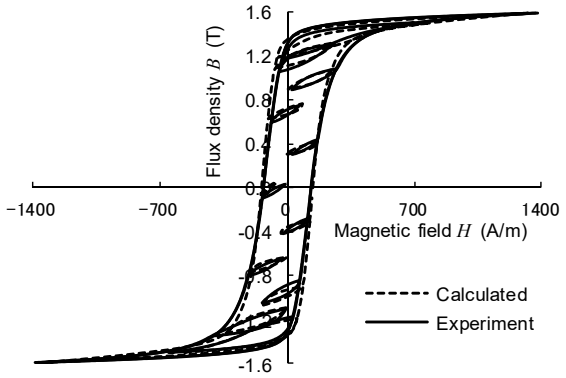

Fig. 5. Experimental verification of hysteresis modeling.

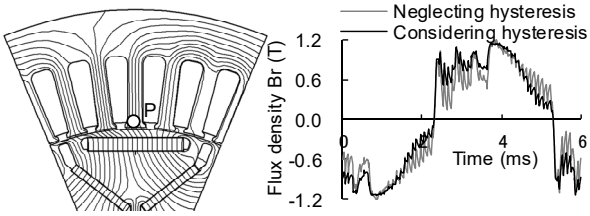

Fig. 6. Calculated flux density waveform (2500 r/min, 88A)

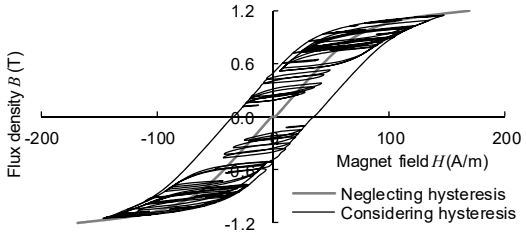

Fig. 7. Calculated hysteresis loop (2500 r/min, 88A).

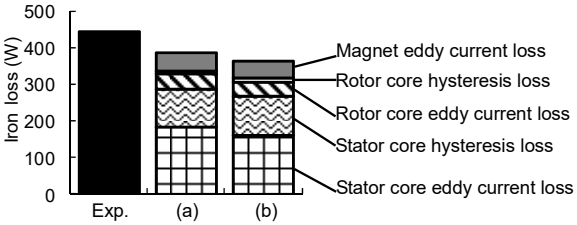

Fig. 8. Experimental and calculated iron losses (2500 r/min, 88A).
(a):Considering hysteresis, (b):Neglecting hysteresis

Reference

1) M. Rekik, O. Hubert, and L. Daniel, "Influence of a multiaxial stress on the reversible and irreversible magnetic behavior of a 3% Si-Fe alloy", *Int. J. Applied Electromagnetics and Mechanics*, vol. 44, no. 3, 4, pp. 301-315, 2014.

2) L. Daniel and O. Hubert, "An equivalent stress for the influence of multiaxial stress on the magnetic behavior," *J. Applied Physics*, vol. 105, 07A313, 2009.

3) K. Yamazaki and Y. Sakamoto, "Electromagnetic field analysis considering reaction field caused by eddy currents and hysteresis phenomenon in laminated cores," *IEEE Trans. Magn.*,vol.59, no. 3, 1300294, 2018.

Homogenization Techniques for Laminated Core and Soft Magnetic Composites in Magnetic Field Analysis

Kazuhiro Muramatsu
Department of Electrical and Electronic Engineering, Saga University, Saga 840-8502, Japan

1. Introduction

In electrical machines, laminated cores and soft magnetic composites (SMCs) are often used in order to reduce the eddy current losses. In the magnetic field analysis of such machines, the cores are usually modeled by solid ones in order to save computation cost. To take account of the nonlinearity and the eddy currents in steel plates or particles, and the gaps between them in the solid core model, homogenization techniques [1), 2)] are applied. In this paper, the homogenization techniques for laminated core and SMCs are described.

2. Homogenization Technique

The flowchart of the homogenization technique for laminated core or SMCs is shown in Fig. 1. The sub-analysis with the cell model of a steel plate or particle is carried out for each element *ie* in the core at each nonlinear iteration in the 3D nonlinear eddy current analysis with the solid core model ("main-analysis"). In the sub-analysis, the flux densities obtained from the main analysis are given and the effective permeability used in the main analysis is calculated taking account of the nonlinearity, the eddy currents, and the gaps.

3. Laminated Core

In the sub-analysis of the homogenization technique for the laminated core, one sheet of steel plate with the gap is chosen as the cell model, shown in Fig. 2, and the 1D nonlinear eddy current analysis is carried out.

The homogenization technique is applied to a simple reactor model [3)] shown in Fig. 3. The cores with gaps are constructed by laminated steel plates (35A270) in the *z*-direction, and the space factor *F* is 0.95.

The flux distributions in the leg in the *y*-*z* plane obtained from the ordinary method, neglecting the eddy currents in the steel plates and gaps between the steel plates, and the proposed method mentioned above are shown in Fig. 4. The flux distribution obtained from the ordinary method is almost uniform in the core, whereas the flux densities in the upper layers of the core are larger than those in the other lower layers in the proposed method. This is because the flux concentrates at the corners of cores due to the gaps between cores and the larger flux in the upper layers remains due to the gaps between the steel plates. Therefore, the proposed method should be used for the accurate

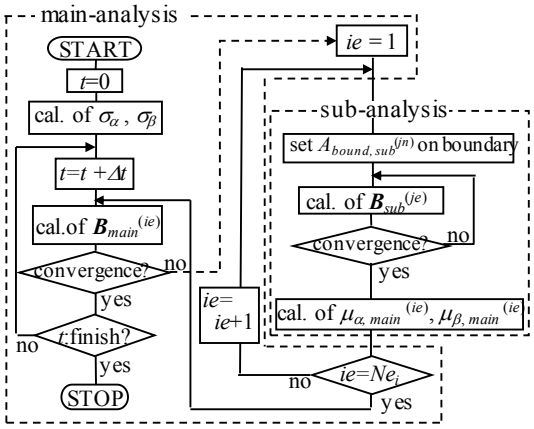

Ne_i : number of elements in core in main-analysis

Fig. 1 Flowchart of homogenization technique.

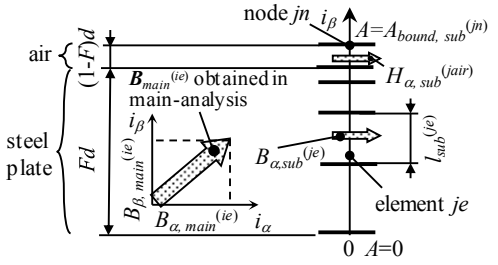

Fig. 2 1D cell model of a steel plate in laminated core.

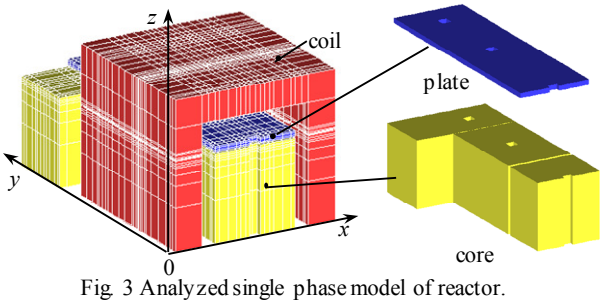

Fig. 3 Analyzed single phase model of reactor.

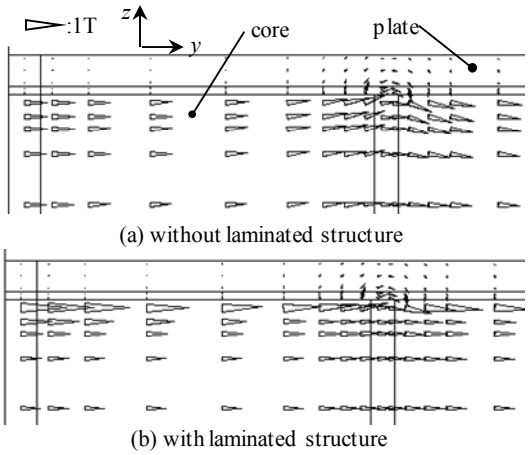

(a) without laminated structure

(b) with laminated structure

Fig. 4 Flux distributions in the leg

analysis of the laminated core.

4. Soft Magnetic Composites (SMCs)

To establish the homogenization technique for SMC, the accurate cell model of a particle with gap is investigated[4]. Fig. 5 shows a 3D cell model for an actual SMC (MBS-R3, DIAMET CORPORATION). In this model, the particles are assumed to be square shape and be formed regularly and infinitely. Two configurations of particles with uniform and un-uniform gaps are examined as shown in Fig. 5 (a) and (b), respectively. In the model with the uniform gap, two gap lengths G_0s are selected. One is G_0s = 1.37 μm determined by volume filling rate. The other is set to be G_0 = 0.35 μm so that the calculated magnetic field H_z coincides with measured one at B_z = 1T. In the non-uniform gap model, G_1, G_2, and L in Fig 1 (b) are optimized to be 0.15, 1.0, and 35 μm so that the calculated BH curve coincides with the measured one as possible.

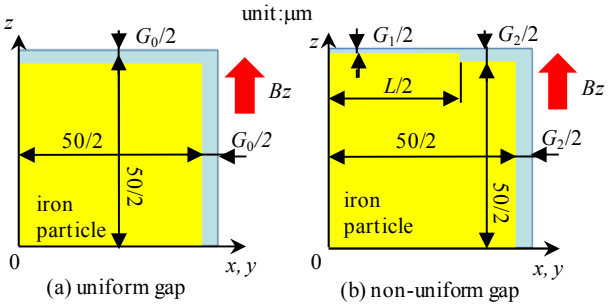

Fig. 5 3D Cell model of a particle in SMC.

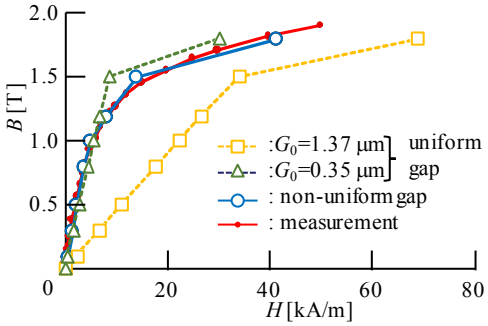

Fig. 6 Calculated and measured initial BH curves.

Fig. 6 shows the calculated and measured effective initial BH curves in the low frequency in which the eddy current can be neglected. In the model with uniform gap G_0 = 1.37 μm, the calculated effective permeability is much smaller than the measured one because the gap length determined by the filling ratio is larger than most of those in the actual SMC due to its complex shape of particles. The model with the smaller uniform gap G_0 = 0.35 μm cannot represent the measured BH curve completely, too. The BH curve obtained by the optimized model with non-uniform gap is good agreement with the measured one. It can be concluded that the cell model with non-uniform gap should be used for the homogenization technique of SMC.

Fig. 7 shows the comparison of the calculated iron losses obtained by using the cell model shown in Fig. 5 (a) with the measred ones. The calculated hysteresis losses are in good agreement with the measured ones because the applied flux density coincides with each other. However, the eddy current losses are different from measured ones because the insulation between particles are not completed in an actual SMCs. This problem will be investigated in future.

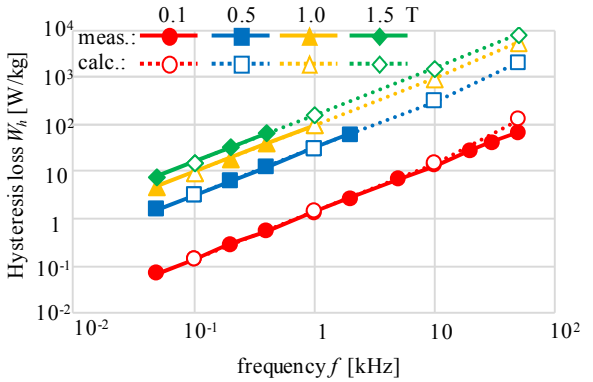

(a) hysteresis loss

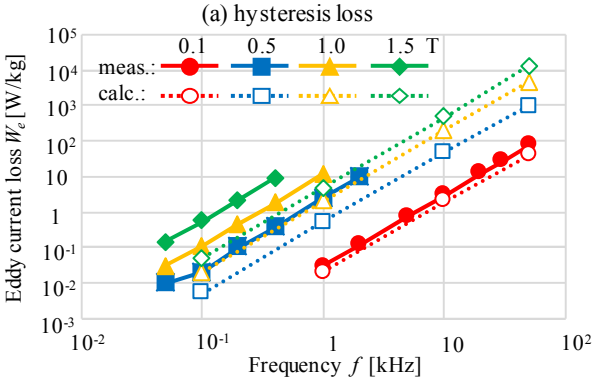

(b) eddy current loss

Fig. 7 Iron losses.

References

1) K. Muramatsu, et al., *IEEE Trans. Magn.*, vol. 40, no. 2, pp. 896-899, 2004.
2) Y. Sato, et al., *IEEE Trans. Magn.*, vol. 53, no. 6, Art. no. 7402204, 2017.
3) Y. Gao, et al., *IEEE Trans. Magn.*, vol. 45, no. 3, pp. 1044-1047, 2009.
4) Y. Gao, et al., *IEEE Trans. Magn.*, vol. 54, no. 3, Art. no. 7401504, 2018.

Magnetic Material Modeling and Simulation Technology for Loss Calculation

A. Furuya, Y. Uehara, K. Shimizu, J. Fujisaki, T. Ataka, T. Tanaka, H. Kawano* and H. Oshima*
(Fujitsu Ltd., *Fujitsu Laboratories Ltd.)

Soft magnetic materials such as an electrical steel, ferrite core, and dust core are widely used in an inductor and transformer. To achieve high efficiency and downsizing, a simulation technology for accurate core loss is highly demanded in the industry. However, core loss is strongly related to complex magnetization dynamics, and magnetic material modeling is one of the recent fields in which progress is being made. In this presentation, we introduce a magnetic material modeling technique based on micromagnetics for electrical steel, and microstructure for ferrite core.

For electrical steel, hysteresis loss accounts for a large portion of core loss of motors. In addition, vector property due to grain structure is observed in B-H loop measurement. To model this property, we adopted a grain magnetics (GM) model[(1)]. Fig. 1 shows the conceptual diagram of the GM model. The magnetization of one grain is approximated by one magnetization vector. This formulation cannot treat a domain-wall and its related dynamics, and therefore, artificial magnetization change such as magnetization flip is introduced. Fig. 2 shows the simulation results for grain-oriented electrical steel. Anisotropic B-H loops are well-reproduced by considering the effect of domain-wall motion and crystal anisotropy.

For high frequency applications, soft ferrite cores are an important material, but these core losses are strongly related to eddy-current, dimensional resonance, and excess loss due to the magnetization dynamics. To evaluate core loss of Mn-Zn ferrite, we studied the magnetic field simulation with the effective permittivity that comes from the microstructure of Mn-Zn ferrite[(2)]. Fig. 3 shows the simulation result of core-size dependence of complex permeability. The core sample with diameter size 12.7 mm has a clear peak in its real part due to the dimensional resonance. In this presentation, we will discuss the comparison of core loss with experimental measurement and loss mechanism.

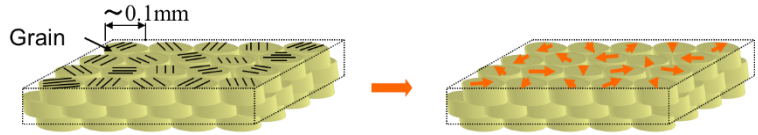

Fig. 1: Grain magnetics model for electrical steel

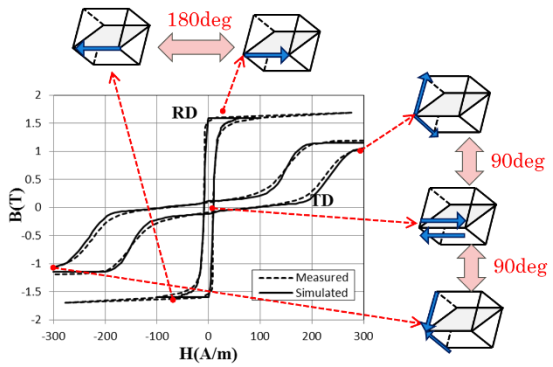

Fig. 2: B-H loops of grain-oriented electrical steel

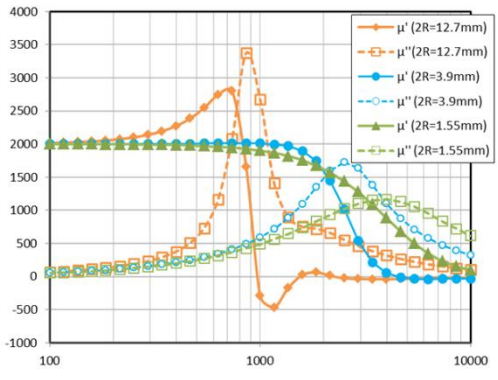

Fig. 3: Complex permeability of Mn-Zn core

Reference

1) A. Furuya,J. Fujisaki,Y. Uehara,K. Shimizu,H. Oshima, and T. Matsuo, IEEE Trans. on Magn., vol. 50,(2014),7300604
2) A. Furuya, Y. Uehara, K. Shimizu, J. Fujisaki, T. Ataka, T. Tanaka and H. Oshima", IEEE Trans. on Magn., vol. 53,(2017), 7301004

Magnetic properties and variational calculus

Fumiaki Ikeda
Photon Co., Ltd.

The finite element method is currently the mainstream method in the field of low frequency electromagnetic field analysis. In this method, Maxwell's equation, which is a fundamental equation, is formulated using a weighted residual method such as the Galerkin method. This is because the magnetization characteristics of magnetic materials are generally not linear with constant magnetic permeability, but have a nonlinear dependence on magnetic flux density.

In the case of a linear magnetic material, the fundamental equation can be expressed as follows using the variational calculus.

$$\delta \int_V [\frac{1}{2\mu}(\mathrm{rot}\boldsymbol{A})^2 - \boldsymbol{J}\cdot\boldsymbol{A}]dV = 0 \tag{1}$$

Here μ is permeability and has a constant value. $\boldsymbol{A}$ is vector potential, and $\boldsymbol{J}$ is current density. Taking variations, the left-hand side becomes as follows.

$$\begin{aligned}&\int_V [\frac{1}{\mu}\mathrm{rot}\delta\boldsymbol{A}\cdot\mathrm{rot}\boldsymbol{A} - \delta\boldsymbol{A}\cdot\boldsymbol{J}]dV \\ &= \int_V \delta\boldsymbol{A}\cdot[\mathrm{rot}\frac{1}{\mu}\mathrm{rot}\boldsymbol{A} - \boldsymbol{J}]dV + \text{(Surface integral)}\end{aligned} \tag{2}$$

However, since the transformation of the last formula was performed using Gauss' theorem, a surface integral has appeared. Since this surface integral normally disappears through boundary conditions, it is required that the integral of the first term be zero, and it is possible to solve the electromagnetic field equation by the variational calculus.

However, in general magnetic materials, the magnetic permeability is not constant, and so such variational calculus cannot be used. Therefore, when dealing with these kinds of magnetic materials using the finite element method, we utilize the vector weighting function $\boldsymbol{W}$ to produce the following equation.

$$\int_V \boldsymbol{W}\cdot[\mathrm{rot}\frac{1}{\mu}\mathrm{rot}\boldsymbol{A} - \boldsymbol{J}]dV = 0 \tag{3}$$

If the left-hand side can be transformed using Gauss' theorem and the surface integral eliminated through boundary conditions, the formula becomes as follows.

$$\int_V [\frac{1}{\mu}\mathrm{rot}\boldsymbol{W}\cdot\mathrm{rot}\boldsymbol{A} - \boldsymbol{W}\cdot\boldsymbol{J}]dV = 0 \tag{4}$$

In this study, we show that the variational calculus can be used even for general magnetic materials by considering the thermodynamics of the magnetic material, and demonstrate that, in electromagnetic field analysis also, the finite element method can be formulated naturally.

Considering the free energy F of the magnetic material as a function of temperature T and magnetic flux density $\boldsymbol{B}$, this differential can be expressed as follows.

$$dF(T,\boldsymbol{B}) = -SdT + \boldsymbol{H}\cdot d\boldsymbol{B} \tag{5}$$

Here, S is the entropy of the magnetic material per unit volume, T is temperature, and $\boldsymbol{H}$ is magnetic field. From this, the thermodynamic variables can be expressed as follows.

$$\begin{aligned}S &= -\frac{\partial}{\partial T}F(T,\boldsymbol{B}) \\ \boldsymbol{H} &= \frac{\partial}{\partial \boldsymbol{B}}F(T,\boldsymbol{B})\end{aligned} \tag{6}$$

Here we introduce the following thermodynamic potential by transforming variables.

$$G(T, \boldsymbol{H}) = F(T, \boldsymbol{B}) - \boldsymbol{H} \cdot \boldsymbol{B} \tag{7}$$

Calculating this derivative, the following is obtained from Eq. (5).

$$dG(T, \boldsymbol{H}) = -SdT - \boldsymbol{B} \cdot d\boldsymbol{H} \tag{8}$$

In electromagnetic field analysis, the magnetic field is often obtained by inputting a current, which corresponds to the problem of finding the magnetic flux density for a magnetic field $\boldsymbol{H}$ generated by an electric current. According to thermodynamics, for fixed temperature and magnetic field, this temperature thermodynamic potential is at its minimum at equilibrium. Therefore, the variation of the following integral must be zero if temperature is constant.

$$\delta \int_V G(T, \boldsymbol{H}) dV = 0 \tag{9}$$

Since temperature and magnetic field are here assumed to be fixed, this variation is taken on magnetic flux density, which is the other state quantity. The variation on the left-hand side of this equation is calculated as follows.

$$\begin{aligned} &\int_V [\frac{\partial}{\partial \boldsymbol{B}} F(T, \boldsymbol{B}) \cdot \delta \boldsymbol{B} - \boldsymbol{H} \cdot \delta \boldsymbol{B}] dV \\ &= \int_V dV \delta \boldsymbol{B} \cdot [\frac{\partial}{\partial \boldsymbol{B}} F(T, \boldsymbol{B}) - \boldsymbol{H}] dV \end{aligned} \tag{10}$$

When the variations are represented by vector potentials,

$$\delta \boldsymbol{B} = \delta \mathrm{rot} \boldsymbol{A} = \mathrm{rot} \delta \boldsymbol{A} \tag{11}$$

The above left-hand side can be further transformed as follows through partial integration using Gauss' integral theorem.

$$\begin{aligned} &\int_V dV \mathrm{rot} \delta \boldsymbol{A} \cdot [\frac{\partial}{\partial \boldsymbol{B}} F(T, \boldsymbol{B}) - \boldsymbol{H}] dV \\ &= \int_V dV \delta \boldsymbol{A} \cdot \mathrm{rot} [\frac{\partial}{\partial \boldsymbol{B}} F(T, \boldsymbol{B}) - \boldsymbol{H}] dV + \text{(Surface integral)} \end{aligned} \tag{12}$$

Since the terms of the surface integral can be eliminated by appropriate boundary conditions, the above equation becomes as follows.

$$\int_V dV \delta \boldsymbol{A} \cdot [\mathrm{rot} \frac{\partial}{\partial \boldsymbol{B}} F(T, \boldsymbol{B}) - \mathrm{rot} \boldsymbol{H}] dV \tag{13}$$

Although the distribution of the magnetic field cannot be determined, the magnetic field within this integral is subject to a rotation operator, and can be converted into current density as follows.

$$\mathrm{rot} \boldsymbol{H} = \boldsymbol{J} \tag{14}$$

Therefore, the equation obtained from the variational calculus for the thermodynamic potential, which is required from thermodynamics, is as follows.

$$\int_V dV \delta \boldsymbol{A} \cdot [\mathrm{rot} \frac{\partial}{\partial \boldsymbol{B}} F(T, \boldsymbol{B}) - \boldsymbol{J}] dV = 0 \tag{15}$$

From equation (6), we can see that this formula is equivalent to the electromagnetic field analysis equation.

Here, by examining the magnetic material thermodynamically, we have shown that magnetization characteristics can be expressed by thermodynamic potentials such as free energy, and that the variational calculus can be used in the finite element method for the electromagnetic field.

Issues of Material Modeling in Electromechanical Simulations

Takashi Yamada[1], Katsuyuki Narita[1], Hiroyuki Sano[1]
([1]JMAG division, JSOL Corp.)

Many electrical devices are re-designed today in the electrification. Since the electrification is mainly for energy saving or the global warming countermeasures, high energy efficiency is primary requirement of the re-design. A typical example is electric motors of electric vehicles which have to have high energy efficiency as well as high power density with which the conventional internal combustion engines must be able to be replaced.

On the other hand, the further improvement is challenging since such electric machines have long history of over 100 years and countless efforts have been already made in the history. In order to make a breakthrough, advanced simulation technologies such as finite element analysis (FEA) has been introduced and recognized as an indispensable tool in the machine developments. Major advantages of FEA are, firstly, virtual prototyping where any design ideas can be concretely implemented and evaluated and, secondly, detail phenomena in a machine are visualized and investigated. Those advantages give us deep insights in a complex system and substantial improvements which are difficult with conventional design approaches consisting of empirical equations and real prototyping.

However, to enjoy the advantages, the simulation has to have enough accuracy. Since main error source of today's FEA is material data, accuracy of the material modeling determines performance of the simulation. Hereafter, we focus on losses of lamination steel which is used for core of the electric machines and its property largely affects the performance of the machines. More importantly, the property of the lamination steel is complex and difficult to be modeled so that we have many remaining issues there.

The losses of the lamination steel consist of hysteresis loss, eddy current loss and excess loss. The hysteresis loss is a loss defined by loops of static BH characteristic, i.g. it is frequency independent. The eddy current loss is caused by the classical eddy current circulating in a cross section which is perpendicular to main linkage flux direction. The excess loss is defined as a difference between total losses and summation of the hysteresis loss and eddy current loss.

Most common modeling approaches for loss evaluation today employ an empirical formula such as Steinmetz's equation in which coefficients and parameters are determined with measurements. The measurements are usually done with a pure sinusoidal waveform of magnetic flux density. Advantages of the conventional approach are, firstly, it is accurate if the actual operating condition is the same as the condition of measurements determining the coefficients of the formula and, secondly, it is simple to use since the total loss is calculated with a single formula which includes all losses in the above.

Disadvantage of the conventional approach is the fact that accuracy is never be guaranteed if the measurement condition does not match to the actual operating condition. Those undesirable situations are not rare in actual machines, especially, in advanced machines such as a traction motor of EVs. Those advanced machines are fed with higher current than of the conventional machines to achieve high power density so that the lamination steel is magnetically highly saturated and this does not satisfy the measurement condition. Also, those advanced machines are controlled with inverter(s) employing Pulse Width Modulation (PWM) technique which generates high frequency minor loops on a fundamental major loop. The measurement condition does not include the minor loops and the resulting losses cannot represent the minor loop losses. The minor loops are generated not only by PWM but also by slot harmonics in a Permanent Magnet Synchronous Machine (PMSM) which is the main stream in EVs. Moreover, the measurement has limitation in frequency which actual frequency in a machine goes above the limitation. The disadvantage was not a significant problem because classical machines are designed to be operated with the low frequency sinusoidal waveforms of magnetic flux density.

To overcome the disadvantage, new models have been introduced for the hysteresis loss and the eddy current loss. The hysteresis loss is represented with Play-Hysteron model[1)] which is a semi-physical model and can reproduce a minor loop at an arbitrary operation point employing multiple static major loops. The eddy current loss is modeled by 1D-FEM[1)] in which eddy current distribution in thickness direction is solved with a conductivity of the steel sheet by one-dimensional FEM at each element of the main 2D/3D FEM. Note that since only conductivity is required, this method is valid for any frequency without limitation. Those two models give us significant improvements in accuracy for the advanced machines[3)]. A significant difference from the conventional approach is the fact that the new approach does not depend on measured losses and has wider applicability than the conventional approach.

However, the new approach misses the excess loss is inaccurate in case the excess loss is not ignorable. Although the best way to incorporate the excess loss is having a physical model, the phenomena are too complex to capture the mechanism. Currently, we are developing an expandable empirical based model as a second best. The new model shows reasonable performance for wide range even outside of the measurements. The detail will be explained in the presentation.

Reference

1) T. Matsuo, D. Shimode, , Y. Terada, M. Shimasaki ,"Application of stop and play models to the representation of magnetic characteristics of silicon steel sheet", IEEE Transactions on Magnetics, vol.39, no.3, pp. 1361-1364, 2003
2) O. Bottauscio, “Advanced Model of Laminated Magnetic Cores for Two-Dimensional Field Analysis”, IEEE Transactions on Magnetics, vol.36, no.3, pp561-573, 200
3) K. Narita, H. Sano, T. Yamada, K. Aiso, K. Akatsu, “An Accurate Iron Loss Evaluation Method Based on Finite Element Analysis for Switched Reluctance Motors”, ECCE 2015

Equivalent circuit for Eddy Current Field in Cauer Form

Y. Shindo[1] and T. Matsuo[2]
[1]Kawasaki Heavy Industries, Akashi 673-8666, Japan
[2]Kyoto University, Kyoto 615-8520, Japan

Recently, an exact and efficient modeling method for the eddy current field is found.[1)] This method expands the eddy current field to an equivalent circuit called Cauer Ladder Network (CLN). The procedure for obtaining this network and the benefits of this method are introduced here.

Consider a magnetic sheet shown in Fig. 1, where d denotes the width of the sheet, μ and σ denote the magnetic permeability and electric conductivity of the material respectively. It is supposed that exciting field $\dot{H}_0$ is applied externally. The equation for the eddy current field is given by (1) as an one-dimensional problem.

$$\frac{\partial^2 \dot{H}(x)}{\partial x^2} - j\omega\sigma\mu\dot{H}(x) = 0 \quad . \tag{1}$$

Solving this equation under the boundary condition $\dot{H}(d/2) = \dot{H}_0$ gives the magnetic field (2) and the equivalent magnetic permeability as (3).

$$\dot{H}(x) = \frac{\cos(kx)}{\cos(kd/2)}\dot{H}_0 \tag{2}$$

$$\dot{\mu} = \frac{\dot{\Phi}}{d\dot{H}_0} = \mu\frac{2}{kd}\tan\left(\frac{kd}{2}\right), \qquad \dot{\Phi} = \int_{-d/2}^{d/2}\mu\dot{H}(x)\,\mathrm{d}x = \frac{2\mu}{k}\tan\left(\frac{kd}{2}\right)\dot{H}_0 . \tag{3}$$

Here the complex variable k is defined by $k = \sqrt{-j\omega\sigma\mu}$ and $\dot{\Phi}$ denotes the total flux in the magnetic sheet. The trigonometric function divided by its argument can be expanded by the following two forms, a partial fraction expansion (4) and a continued fraction (5).

$$\frac{1}{z}\tan z = -2\sum_{n=1}^{\infty}\frac{1}{z^2 - \left[(2n-1)\pi/2\right]^2} \tag{4}$$

$$\frac{1}{z}\tan z = \cfrac{1}{1-\cfrac{z^2}{3-\cfrac{z^2}{5-\cfrac{z^2}{7-\cfrac{z^2}{9-\cdots}}}}} \tag{5}$$

By setting $R_c = 8/\sigma d^2$, $L_c = \mu$ and $L_{cn} = 2L_c/(n-1/2)^2\pi^2$, the effective complex permeability can be respectively expanded as

$$j\omega\dot{\mu} = \sum_{n=1}^{\infty}\frac{j\omega L_{cn}R_c}{R_c + j\omega L_{cn}} \tag{6}$$

$$j\omega\dot{\mu} = \cfrac{1}{1/j\omega L_c + \cfrac{1}{3(R_c/2) + \cfrac{1}{5/j\omega L_c + \cfrac{1}{7(R_c/2) + \cdots}}}} . \tag{7}$$

The former corresponds to the Fourier I expansion and the latter corresponds to the Cauer I expansion. The equivalent circuits for these expansions can be realized by the equivalent circuits shown in Fig. 2, Foster realization and Cauer realization respectively. These equivalent circuits can be employed for modeling of actual electric machines such as a reactor as shown in Fig. 3. In fact, the reactance of this reactor is expressed by $\mathrm{j}\omega L = \mathrm{j}\omega\dot{\mu}SN/l$, where S, N and l

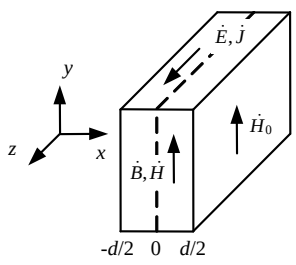

Fig. 1. Magnetic sheet

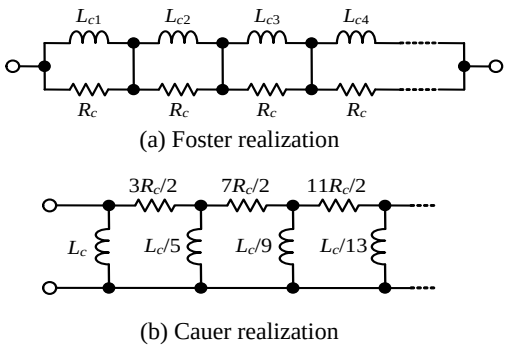

(a) Foster realization

(b) Cauer realization

Fig. 2. Equivalent circuits

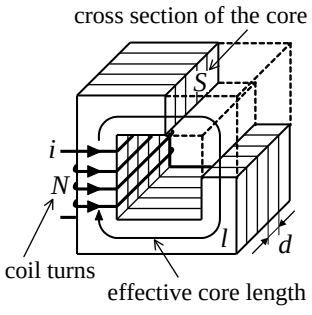

Fig. 3 Reactor

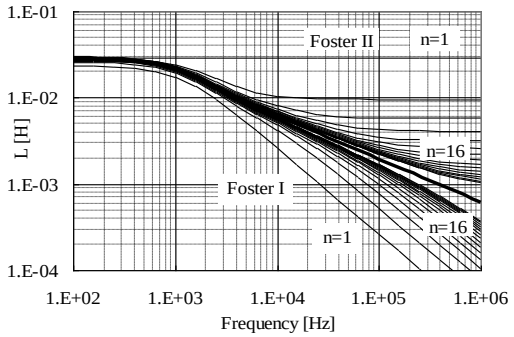

(a) Foster I and II

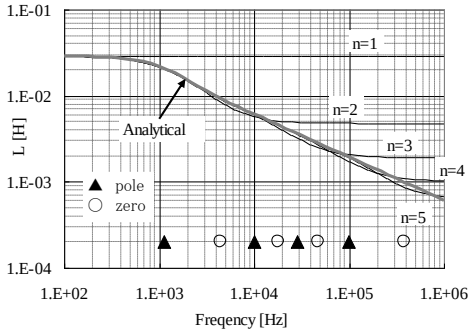

(b) Cauer I

Fig. 4. Bode plots of Foster and Cauer expansions. ($L = \dot{\mu}$)

denote the cross section of the laminated core, the coil turns and the effective core length respectively. The examples of Bode plots with finite truncations of these networks are shown in Fig 4, where *n* denotes the number of the inductors. It is obvious that Cauer expansion is much effective than Foster expansion.

Recently, it was found that this Cauer realization can be expanded to arbitrary three-dimensional eddy current field as illustrated in Fig. 5.[2] For preparation, define

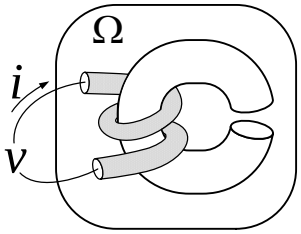

Fig. 5. Eddy current field

$$\boldsymbol{E} = \sum_{n=0}^{\infty} e_{2n}\bar{\boldsymbol{E}}_{2n}, \quad \boldsymbol{H} = \sum_{n=0}^{\infty} h_{2n+1}\bar{\boldsymbol{H}}_{2n+1}, \tag{8}$$

$$1/R_{2n} = \int_{\Omega} \sigma \bar{\boldsymbol{E}}_{2n} \cdot \bar{\boldsymbol{E}}_{2n} \mathrm{d}V, \quad L_{2n+1} = \int_{\Omega} \mu \bar{\boldsymbol{H}}_{2n+1} \cdot \bar{\boldsymbol{H}}_{2n+1} \mathrm{d}V . \tag{9}$$

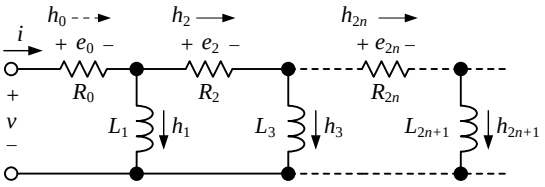

Fig. 6. Ladder network

Then the method is presented by the following steps.

***Step* 0**: Assume that the voltage *v* is applied externally. Solve $\nabla \times \boldsymbol{E}_0 = 0$ under given voltage boundary condition. Set $\bar{\boldsymbol{E}}_0 = \boldsymbol{E}_0 / v$ and calculate R_0 using (9). Set $\bar{\boldsymbol{H}}_{-1} = 0$ and n = 1.

***Step* 1**: Solve $\nabla \times \tilde{\boldsymbol{H}}_{2n-1} = R_{2n-1}\sigma \bar{\boldsymbol{E}}_{2n-2}$ under magnetic boundary conditions. Set $\bar{\boldsymbol{H}}_{2n-1} = \tilde{\boldsymbol{H}}_{2n-1} + \bar{\boldsymbol{H}}_{2n-3}$ and calculate L_{2n-1} by using (9).

***Step* 2**: Solve $\nabla \times \tilde{\boldsymbol{E}}_{2n} = -(1/L_{2n-1})\mu \bar{\boldsymbol{H}}_{2n-1}$. Set $\bar{\boldsymbol{E}}_{2n} = \tilde{\boldsymbol{E}}_{2n} + \bar{\boldsymbol{E}}_{2n-2}$ and calculate R_{2n} by using (9).

***Step* 3**: If the finite sum of (8) converge sufficiently, then stop the calculation. Otherwise set $n = n+1$ and go to ***Step* 1**.

This method provides the network constants in Fig. 6, and simultaneously provides the spatial distribution functions $\bar{\boldsymbol{E}}_{2n}$ and $\bar{\boldsymbol{H}}_{2n+1}$. The circuit variables e_{2n} and h_{2n+1} can be obtained by real-time simulation of the ladder network. The magnetic field and the current distribution can be synthesized using (8). Furthermore, the total magnetic energy W_m and the power consumption W_R in the entire domain Ω are presented in lumped forms as

$$W_m = \frac{1}{2}\sum_{n=0}^{\infty} L_{2n+1} h_{2n+1}^2, \quad W_R = \sum_{n=0}^{\infty} R_{2n} \left(\sum_{m=n}^{\infty} h_{2n+1} \right)^2 . \tag{10}$$

In the actual electric machine designs, the nonlinearity and hysteresis property, as well as the anomaly eddy current loss, frequently become important issues. [3] The authors hope that the proposed method can be applied to estimate the anomaly eddy current loss. However, it may not be so easy because of the moving of domain walls due to the fluctuation of the magnetic field.

Reference

1) Y. Shindo *et al*., Simple Circuit Simulation Models for Eddy Current in Magnetic Sheets and Wires, IEEJ Trans. FMS, Vol. 134, Issue 4, pp.173-181 (2014)
2) A. Kameari *et al*., Cauer Ladder Network Representation of Eddy-Current Fields for Model Order Reduction Using Finite-Element Method, IEEE Tran MAG, Vol. 52, Issue 3, #7201804 (2018)
3) G. Bertotti, Hysteresis in Magnetism, Academic Press (1998).